

1

2 **Study on the COP of Free Piston Stirling Cooler**  
3 **(FPSC) in the anti-sublimation CO<sub>2</sub> capture process**

4

5 Chunfeng Song <sup>a,\*</sup>, Jingwen Lu <sup>b</sup>, Yutaka Kitamura <sup>b</sup>

6

7 *<sup>a</sup> School of Environmental Science and Engineering, Tianjin University, Tianjin*  
8 *300072, China*

9 *<sup>b</sup> Graduate School of Life and Environmental Sciences, University of Tsukuba, 1-1-1,*  
10 *Tennodai, Tsukuba, Ibaraki 305-8572, Japan*

11

12

13

14

15

16 \* Corresponding author. Tel.: +81 0298-53-4655; Fax: +81 0298-53-4655.

17 E-mail address: [songcf@iis.u-tokyo.ac.jp](mailto:songcf@iis.u-tokyo.ac.jp)

18

19

20

21

22 **Abstract**

23 Free piston Stirling cooler (FPSC) is a promising alternative for the conventional  
24 coolers and has been applied to various fields. In the previous research, a novel  
25 cryogenic CO<sub>2</sub> capture system based on FPSCs has been exploited. In order to  
26 enhance the cryogenic CO<sub>2</sub> capture efficiency, the investigation on the coefficient of  
27 performance (COP) of the FPSC is carried out in this work. In detail, the influence of  
28 different materials (aluminium and copper), size of cold head (length and diameter),  
29 as well as ambient conditions (humidity and temperature) on the COP of the  
30 cryogenic system were tested. The experiment results indicate that the material of cold  
31 head should be selected at copper to increase the COP of CO<sub>2</sub> capture system. The  
32 length and diameter of cold head should be short and thick. In addition, the low  
33 ambient temperature is benefit for the high COP. For the optimal conditions ( the  
34 material was copper, length and diameter were 180 and 40 mm, respectively), the  
35 temperature of the cold head reached -140 °C, and the COP of the FPSC and the  
36 cryogenic CO<sub>2</sub> system was 0.82 and 0.70, respectively.

37

38

39 *Keywords:* free piston Stirling cooler, COP, performance, CO<sub>2</sub> capture

40

41

42

|                     |
|---------------------|
| <b>Nomenclature</b> |
|---------------------|

|     |                         |
|-----|-------------------------|
| $L$ | Length of cold head, mm |
|-----|-------------------------|

|                      |   |
|----------------------|---|
| $P$                  | Pressure, Pa                            |
| $Q$                  | Cooling capacity, J                     |
| $T_a$                | Ambient temperature, °C                 |
| $T_c$                | Temperature of the cold head, °C        |
| $V$                  | Volume, m <sup>3</sup>                  |
| $W$                  | Input power, J                          |
| $h_a$                | Ambient humidity, %                     |
| $m$                  | Mass, kg                                |
| <i>Abbreviations</i> |   |
| <i>CCS</i>           | CO <sub>2</sub> capture and storage     |
| <i>COP</i>           | Coefficient of performance              |
| <i>FESC</i>          | Free piston Stirling cooler             |
| <i>LN2</i>           | Liquid nitrogen                         |
| <i>LNG</i>           | Liquefied natural gas                   |
| <i>PCC</i>           | Post-combustion CO <sub>2</sub> capture |

43

44

45

46

47

48 **1. Introduction**

49 According to the prediction of Intergovernmental Panel on Climate Change (IPCC),  
50 by the year 2100, the atmosphere may contain up to 570 ppmv of CO<sub>2</sub>, causing a rise  
51 of mean global temperature of around 1.9 °C and an increase in mean sea level of 3.8  
52 m [1]. As an effective strategy to mitigating CO<sub>2</sub> emissions, much attention has been  
53 paid on post combustion CO<sub>2</sub> capture (PCC) techniques. Nowadays, the most mature  
54 post-combustion CO<sub>2</sub> capture technology is based on CO<sub>2</sub> absorption by aqueous  
55 amine solutions and has been commercially utilized on the large CO<sub>2</sub> emission  
56 sources (i.e. coal-fired power plants, cement and steel plant) [2,3]. In the absorption  
57 processes, CO<sub>2</sub> reacts reversibly in an absorber with amines which are regenerated by  
58 heating the solution in a stripper column [4]. Nevertheless, the biggest bottleneck for  
59 the chemical absorption processes is that the regeneration of solvents is energy  
60 penalty [5,6]. Meanwhile, the degradation of the aqueous amine solvents also leads to  
61 an increasing cost [7]. In light of this situation, the alternative methods (such as  
62 adsorption, membrane, cryogenic, microalgae and chemical looping) have also  
63 attracted the attention of the scientists [8]. Compared to the other CO<sub>2</sub> capture  
64 technologies, cryogenic CO<sub>2</sub> capture approach can achieve a high CO<sub>2</sub> purity (above  
65 99%) and which can minimize the compression and transport costs significantly [9].  
66 Furthermore, the CO<sub>2</sub> capture process can be achieved by the phase change, and there  
67 is no utilization of chemical solvents. Consequently, a number of researches have  
68 been driven toward this technique. [10-13].

69 As the critical part of the cryogenic CO<sub>2</sub> capture methods, several low temperature  
70 sources have been utilized and investigated [14]. In 2002, Clodic et al. developed a

71 novel cryogenic CO<sub>2</sub> capture process by using the cold duty from liquid nitrogen  
72 (LN<sub>2</sub>). The CO<sub>2</sub> in the flue gas can be recovered in the liquid form and which is  
73 beneficial to the further compression and transport. However, the main disadvantage  
74 of the process is that the deposited CO<sub>2</sub> on the cold head would adversely affect the  
75 heat transfer. Moreover, the moisture in the flue gas has to be separated beforehand to  
76 avoid the plugging by ice during the operation [15]. In 2011, Tuinier et al. exploited a  
77 cryogenic packed bed taking advantage of the cold energy from liquefied natural gas  
78 (LNG) regasification terminal. The moisture and CO<sub>2</sub> can be separated and collected  
79 at the different locations in the process. However, the coefficient of performance  
80 (COP) of the system is typically 0.5, and thus about 3.6 MJ electric energy is required  
81 and resulting in even higher thermal energy to capture per kg CO<sub>2</sub> [16].

82 Free piston Stirling cooler (FPSC) is a new type cryogenic cooler attracting interest  
83 as the low temperature source [17]. Compared to the conventional coolers, FPSC can  
84 use helium as regenerator, and avoid the increasing environmental issues (such as  
85 ozone depletion) caused by CFCs, HCFCs and HFCs [18]. Meanwhile, high energy  
86 efficiency and reliability are also the advantage of FPSC. For these reasons, FPSC has  
87 been utilized in the cryogenic CO<sub>2</sub> capture process in the previous work [19].  
88 However, it needs to point out that the original cooling region of FPSC is limit duo to  
89 the size of itself. During the application process, it often needs to extend the cold head  
90 for further refrigeration. Therefore, the investigation on the COP and cryogenic  
91 temperature of FPSC is significant for improving the CO<sub>2</sub> capture efficiency.

92 The objective of this study is to investigate the characteristic of FPSC and

93 theoretically analyze the COP of the FPSC. The research also focuses on the influence  
94 of the key parameters on the COP of FPSC, such as the material (aluminium and  
95 copper) and size (length and diameter) of the cold head, as well as the ambient  
96 conditions (temperature and humidity). The structure of this paper is as follows.  
97 Section 2 describes the cryogenic CO<sub>2</sub> capture process and deduces the COP of FPSC.  
98 Section 3 shows the detailed experimental conditions. Section 4 investigates the key  
99 parameters that influence the COP and cryogenic temperature of FPSC. Section 5  
100 discusses the possibility of increasing the efficiency by the heat exchange between the  
101 separated and incoming streams and the application in the large scale. Section 6  
102 summarizes the main conclusions of this research.

## 103 **2. Base case description**

### 104 *2.1. Cryogenic CO<sub>2</sub> capture process*

105 The structure of designed cryogenic CO<sub>2</sub> capture system based on free piston  
106 Stirling coolers (FPSC) has been introduced in our previous work [20, 21]. The whole  
107 capture process can be briefly described as follows: three Stirling coolers used in the  
108 system are named as FPSC-1, FPSC-2 and FPSC-3, respectively. First, the flue gas is  
109 introduced into the pre-freezing tower. Under the low temperature, the moisture in the  
110 gas stream can condense and be separated. Then the dry flue gas flows into the main  
111 freezing tower. Under the cryogenic condition (approximately -110 °C), the CO<sub>2</sub> in  
112 the gas stream frosts on the surface of the cold head of FPSC-2, and simultaneously  
113 the other gas (such as N<sub>2</sub> and O<sub>2</sub>) is exhausted without phase change. Finally, the

114 captured CO<sub>2</sub> is separated by the motor driven scraper and gathered in the storage  
115 column to further compress for transport. The key parameters (such as flow rate,  
116 temperature and operating time) that affect the capture performance are controlled and  
117 recorded by the control panel.

118 In addition, the detailed connection of FPSC-2, cold head and main-freezing tower  
119 is shown in Fig. 1. The cold head is chilled by FPSC-2 to generate the required low  
120 temperature condition (around -110 °C) in the main freezing tower. Therefore, during  
121 the capture process, the CO<sub>2</sub> in the gas stream can be separated and frosted on the  
122 surface of the cold head. It should be noted that in order to enhance the heat transfer  
123 efficiency, the vacuum interlayer is maintained between the internal of the tower and  
124 the ambient surroundings.

## 125 *2.2. Free piston Stirling cooler (FPSC)*

### 126 *2.2.1 Theoretical analysis*

127 A schematic diagram of the FPSC is shown in Fig. 2. The FPSC may be defined as  
128 a pressure vessel which operates by shuttling approximately 1 gram of helium back  
129 and forth by the combined movements of two parts, namely the piston and the  
130 displacer. While the piston that compresses the gas is driven by a linear motor, the  
131 displacer is moved by the pressure difference. Heat exchanger and regenerator are  
132 assembled to separate the compression and expansion spaces for the creation of a  
133 thermal gradient which allows the FPSC to extract heat from the cold head and reject  
134 heat to the region around hot head. This process is repeated many times per second

135 and can ultimately produce temperature differences between the cold and hot head.  
 136 During the whole process, heat can be moved from a remote location to the FPSC and  
 137 then rejected to the environment. The detailed working principle of FPSC has been  
 138 introduced by Berchowitz in 1992 [22].

### 139 2.2.2 Coefficient of performance (COP)

140 As an important quality to evaluate the performance of FPSC, the investigation on  
 141 the COP is significant. The COP is defined as the ratio of the cooling capacity ( $Q_e$ )  
 142 and the input power ( $W$ ) of the system, and can be expressed as follows:

$$143 \quad COP = \frac{Q_e}{W} \quad (1)$$

144 where the input power ( $W$ ) can be obtained from:

$$145 \quad W = \frac{\omega_0}{2\pi} \int_0^{2\pi} P_c dV \quad (2)$$

146 here  $P_c$  and  $V$  are the pressure and volume of cylinder, and can be given by the  
 147 following equations [22]:

$$148 \quad P_c = \langle P \rangle + |P_c| \sin\phi \quad (3)$$

$$149 \quad V = V_0 - A_p X_p \sin\phi \quad (4)$$

150 Taking equation (3) and (4) into equation (2), the input power ( $W$ ) can be expressed  
 151 as:

$$152 \quad W = -\frac{\omega_0}{2} \alpha_T X_p X_d \sin\phi \quad (5)$$

153 where,  $X_d$  and  $X_p$  are the amplitude of the displacer and piston.  $\alpha_T$  is the thermal  
 154 coupling between the displacer motion and piston force, and it can be calculated as  
 155 follows:



156 
$$\alpha_T = A_p \frac{\partial P_c}{\partial X_d} \quad (6)$$

157 In addition, the cooling capacity ( $Q_e$ ) is described as follows:

158 
$$Q_e = -\frac{\omega_0}{2} \left\{ \alpha_p X_p \left( \frac{A}{A_R} - 1 \right) \sin\phi - K_{ext_d} X_p \frac{A}{A_R} \frac{m_p}{m_c} \sin\phi + C_{ext} \omega_0 X_d \right\} X_d \quad (7)$$

159 where  $A$  is the crosscut area of the cylinder.  $C_{ext}$  is incidental damping. It should be  
 160 noted that heat transfer losses ( $Q_L$ ) is inevitable. Among the heat losses, conduction  
 161 ( $Q_{cond}$ ) and regenerator ( $H$ ) losses are the most significant.

162 
$$Q_L = Q_{cond} + H \quad (8)$$

163 In conclusion, the COP of the FPSC can be expressed as the following equation:

164 
$$COP = \frac{\alpha_p}{\alpha_T} \left( \frac{A}{A_R} - 1 \right) - \frac{A}{A_R} \frac{K_{ext}}{\alpha_T} \frac{m_p}{m_c} + \frac{C_{ext}}{\alpha_T} \frac{\omega_0}{\sin\phi} \frac{X_d}{X_p} \quad (9)$$

165 Simultaneously, the investigation on the coefficient of performance for the whole  
 166 system (COPS) is implemented to evaluate the performance of the system. The COPS  
 167 of the system can be calculated as follows:

168 
$$COPS = \frac{Q_{C1} + Q_{C2} + Q_{C3}}{W_s} \quad (10)$$

169 here  $Q_{C1}$ ,  $Q_{C2}$  and  $Q_{C3}$  are the cooling capacity of FPSC-1, 2 and 3, respectively.  $W_s$  is  
 170 the input energy of the system.

### 171 **3. Experimental**

172 The investigation of the COP are based on the experiments four parameters, namely  
 173 material, length and diameter of the cold head, as well as the ambient humidity and  
 174 temperature. Initially, the cold head of FPSC is tested with different materials  
 175 (aluminium and copper). Then, the size (length and diameter) of the cold head is

176 investigated. The structure of the cold head with different materials (aluminium and  
177 copper) is shown in Fig. 3. The length (L) of cold head is set at (180 mm and 270  
178 mm), respectively. The diameter (D) of the cold head is investigated under 30 mm and  
179 40 mm. It needs to point out that the selection of length and diameter is just  
180 depending on the configuration of the system, and there is no special representation.  
181 Additionally, during the operating process, the FPSC needs to intake the air from  
182 ambient and exhaust the hot air simultaneously. Therefore, the influence of ambient  
183 humidity ( $h_a$ ) and temperature ( $T_a$ ) on the COP of FPSC is also investigated.

## 184 **4. Results**

### 185 *4.1 Effect of the cold head on the COP*

#### 186 *4.1.1 Material*

187 The relationship between the COP of FPSC and the material of the cold head is  
188 investigated according with the chilling process (as shown in Fig. 4). With the  
189 temperature reduction of the cold head, the cooling capacity of FPSC decreased, and  
190 which led to the fall of COP. However, the aluminium cold head has a relative higher  
191 COP decreasing rate compared to the copper one. It results that the FPSC with an  
192 aluminium cold head has a lower COP than the copper one in the whole temperature  
193 drop process. When the root temperature of the cold head dropped to  $-140\text{ }^{\circ}\text{C}$ , the COP  
194 of FPSC with the aluminium and copper cold head are 0.61 and 0.82 respectively. It  
195 can be deduced that the COP of the copper cold head is higher than the aluminium,  
196 and which means a large cooling capacity can be obtained.

197 The effect of the material of cold head on the cryogenic temperature is depicted in  
198 Fig. 5. From the results, it can be concluded that the cold head made by copper has a  
199 lower temperature than aluminium. After 240 min, the root temperatures are  $-111.2\text{ }^{\circ}\text{C}$   
200 for the aluminium cold head and  $-111.3\text{ }^{\circ}\text{C}$  for the copper. Meanwhile, the front  
201 temperatures of the aluminium and copper cold head are  $-78.09\text{ }^{\circ}\text{C}$  and  $-97.82\text{ }^{\circ}\text{C}$ . In  
202 addition, the temperature decreasing rate for the copper cold head is higher than the  
203 aluminium. For copper, the temperature drop from the root of the cold head to the  
204 front is  $13.38\text{ }^{\circ}\text{C}$ . By contrast, although the mass of the cold head by aluminium is  
205 light, the thermal loss is great (with a temperature drop of  $33.31\text{ }^{\circ}\text{C}$ ).

#### 206 *4.1.2 Length*

207 The results in Fig. 6 show that the influence of the length of cold head on the COP  
208 of FPSC. It can be observed that with the increase of the length, the COP of FPSC  
209 decreased obviously. However, for the aluminium cold head, the decreasing rate of  
210 COP is higher than the copper one. When the length is extended from 180 mm to 270  
211 mm, the COP dropped from 0.82 down to 0.59 (the root temperature of the cold head  
212 was  $-140\text{ }^{\circ}\text{C}$ ). It can be explained by the fact that along with the increasing of the  
213 length of the cold head, the heat loss also increase and the cooling capacity of the cold  
214 head reduced accordingly. Therefore, the COP of FPSC also dropped.

215 As the results in Fig. 7, the cryogenic temperature of the cold head decreases with  
216 the extension of the length. When the length of the cold head is set at 180 mm, the  
217 temperature drop from the root to the front is  $9.92\text{ }^{\circ}\text{C}$ . However, with the length

218 extending to 270 mm, the temperature drop rose up to 15.73 °C. Furthermore, after  
219 240 min, the front temperature of the cold head for 180 mm and 270 mm are  
220 -84.08 °C and -73.17 °C. That is because that along with the extension of the length,  
221 the temperature loss of the cold head also increases.

#### 222 *4.1.3 Diameter*

223 As presented in Fig. 8, the COP variation process with different diameters was  
224 investigated. The COP of FPSC reduced according with the temperature drop of the  
225 cold head. With the expanding of the diameter of the cold head (from 30 mm to 40  
226 mm), the COP of FPSC increased obviously. Meanwhile, the decreasing rate of the  
227 COP was decelerated. When the root temperature of the cold head decreased to  
228 -140 °C, the COP was 0.52 (diameter of 30mm) and 0.59 (diameter of 40 mm),  
229 respectively.

230 In addition, the relationship between the diameter and cryogenic temperature of the  
231 cold head was depicted in Fig. 9. From the results, it can be concluded that a large  
232 diameter is beneficial to reduce temperature loss. When the diameter of the cold head  
233 is set at 30 mm, the lowest temperature for the root and front of the cold head is  
234 -85 °C and -64.72 °C. The temperature drop is 20.28 °C from the root to the front side.  
235 By contrast, when the diameter is set at 40 mm, the lowest temperature for the root  
236 and front sides is -88.9 °C and -73.17 °C respectively. The temperature drop can be  
237 reduced to 15.73 °C. For the larger diameter (40 mm), both of the root and front  
238 temperature are lower than the smaller one (30 mm). It indicated that expanding the

239 diameter of the cold head is beneficial to improve heat transfer efficiency and the  
240 COP of FPSC.

#### 241 *4.2 Effect of the ambient conditions on the COP*

242 The effect of ambient temperature on the COP of FPSC is summarized in Fig. 10.  
243 From the result, it can be observed that the COP of FPSC increased with the  
244 decreasing of ambient temperature. When the ambient temperature varied from 8 °C  
245 to 28 °C, the COP of FPSC reduced from 0.7 to 0.6. That is for the reason that during  
246 the refrigeration process of FPSC, it absorbs cool air from surrounding and  
247 simultaneously exhausts warm air. A low ambient temperature is favor of increasing  
248 temperature difference from the cold head of FPSC to the warm side. Thus, in order to  
249 improve the performance of FPSC, the ambient temperature should be dropped as low  
250 as possible. The influence of ambient humidity on the COP of FPSC is shown in Fig.  
251 11. From the results in the figure, it shows that with the ambient humidity increasing  
252 from 20 % to 75 %, the COP of FPSC varied in the range of 0.62 to 0.68. It indicated  
253 that the influence of ambient humidity on the COP of FPSC is not significant.

#### 254 *4.3 COP of the cryogenic CO<sub>2</sub> capture system*

255 The COP variation of the FPSCs (FPSC-1, 2 and 3) and the whole system is shown  
256 in Fig. 12. From the results, it can be found that the COPs of three FPSCs were  
257 different. That is for the reason that due to the different functions in the cryogenic  
258 CO<sub>2</sub> capture system, the length of the cold head of the FPSCs is also different. When  
259 the temperature of the cold head for FPSC-2 was cooled to -140 °C, the COPs of

260 FPSC-1, 2 and 3 were 0.82, 0.78 and 0.79, respectively. Meanwhile, due to the other  
261 energy consumption units (such as vacuum pump, control panel and scraper), the COP  
262 of the whole system was 0.70.

## 263 **5. Discussion**

264 The COP of the Stirling cooler and the developed cryogenic CO<sub>2</sub> capture system  
265 has been tested under various conditions (including material, length and diameter of  
266 the cold head, as well as the ambient temperature and humidity) to achieve the  
267 optimal performance of the system. Simultaneously, the temperature of the cold head  
268 was also investigated to evaluate the cryogenic performance of the Stirling cooler. It  
269 can be concluded that the COP of the Stirling cooler is higher (about 0.82 at -140 °C)  
270 than the common refrigerators (around 0.5 at -140 °C).

271 Although the cryogenic CO<sub>2</sub> capture process has several advantages, it still suffers  
272 some limitations need to be overcome. It should be noticed that the whole capture  
273 process is based on the low temperature condition, and thus the latent heat associated  
274 with the separated components (i.e. the condensate water, exhaust gas and especially  
275 captured CO<sub>2</sub>) would be substantial. For the future work, the cold energy of these  
276 components should be recovered by the heat exchangers, and then the total energy  
277 consumption of the system could be further reduced.

278 Owing to the flow rate of flue gas in the real power plants is higher than the  
279 laboratory scale, the scaling up of the capture capacity of the system is very  
280 significant. It can be achieved by utilizing the high power Stirling coolers. Meanwhile,

281 more Stirling coolers can be integrated into the system to improve the chilling ability  
282 of each parts (such as pre-freezing, main freezing and storage towers). However, it  
283 should be pointed out that with the increase of the amount of the Stirling coolers, the  
284 phenomenon of oscillation of the system may become increasing serious. Therefore,  
285 the influence of the oscillation phenomenon on the COP of Stirling cooler should be  
286 studied in the future research.

## 287 **6. Conclusion**

288 In the present work, the investigation on the COP of the FPSC was carried out. In  
289 order to improve the COP of FPSC in the cryogenic CO<sub>2</sub> capture process, the key  
290 parameters (material, length and diameter of the cold head, as well as the ambient  
291 temperature and humidity) were also investigated. Based on the experimental results,  
292 the conclusions are summarized as follows:

293 1) From the experiment of the materials, it can be concluded that when the cold  
294 head was made by copper, the COP of FPSC was 0.82 with -140 °C of the cold head.  
295 By contrast, the COP of FPSC for the aluminium cold head was 0.61.

296 2) For the different lengths of the cold head (270 mm and 180 mm), the COP of  
297 FPSC was 0.59 and 0.82, respectively. Furthermore, when the diameter of the cold  
298 head was set at 30 mm, the COP of FPSC was 0.52. By contrast, with the diameter  
299 thickening to 40 mm, the COP of FPSC increased to 0.59.

300 3) In addition, the ambient temperature also presented a significant influence on the  
301 COP of FPSC. When the ambient temperature varied from 8 °C to 28 °C, the COP of

302 FPSC reduced from 0.7 to 0.6. Nevertheless, the effect of ambient humidity on the  
303 COP is not significant. With the ambient humidity increasing from 20 % to 75 %, the  
304 COP of FPSC varied in the range of 0.62 to 0.68.

305 4) Although the FPSCs in the system had high COPs, the COP of the system was  
306 around 0.70 due to other energy consumption units (such as vacuum pump and control  
307 panel).

## 308 **Acknowledgement**

309 We thank Mr. Yamano and Mr. Yamasaki of Tanabe Engineering Corporation for  
310 their technological assistance.

## 311 **References**

312 [1] IPCC. Summary for policymakers. In: climate change 2007: the physical science basis,  
313 contribution of working group I to the fourth assessment report of the intergovernmental panel  
314 on climate change. Geneva: World Meteorological Organization/United Nations Environment  
315 Program; 2007.

316 [2] Abu-Zahra MRM, Schneiders LHJ, Niederer JPM, Feron PHM, Versteeg GF. CO<sub>2</sub> capture  
317 from power plants Part I. A parametric study of the technical performance based on  
318 monoethanolamine. Int. J. Greenhouse Gas Control 2007;1:37-46.

319 [3] Versteeg P, Rubin ES. A technical and economic assessment of ammonia-based  
320 post-combustion CO<sub>2</sub> capture at coal-fired power plants. Int. J. Greenhouse Gas Control.  
321 2011;5:1596-1605.



- 322 [4] Gouedard C, Picq D, Launay F, Carrette PL. Amine degradation in CO<sub>2</sub> capture. I. A review.  
323 Int. J. Greenhouse Gas Control. 2012;10:244-270.
- 324 [5] Luis P, Gerven TV, Bruggen BV. Recent developments in membrane-based technologies for  
325 CO<sub>2</sub> capture. Progress in Energy and Combustion Science. 2012;38:419-448.
- 326 [6] Lee ZH, Lee KT, Bhatia S, Mohamed AR. Post-combustion carbon dioxide capture: Evolution  
327 towards utilization of nanomaterials. Renewable & Sustainable Energy Reviews  
328 2012;16:2599-2609.
- 329 [7] Dumé L, Scholes C, Stevens G, Kentish S. Purification of aqueous amine solvents used in  
330 post combustion CO<sub>2</sub> capture: A review. Int. J. Greenhouse Gas Control 2012;10:443-455.
- 331 [8] Rubin ES, Mantripragada H, Marks A, Versteeg P, Kitchin J. The outlook for improved carbon  
332 capture technology. Progress in Energy and Combustion Science 2012;38:630-671.
- 333 [9] Belaïssaoui B, Moullec YL, Willson D, Favre E. Hybrid membrane cryogenic process for  
334 post-combustion CO<sub>2</sub> capture. J. Membrane Sci 2012;415-416:424-434.
- 335 [10] Clodic D, Younes M, Bill A. Test results of CO<sub>2</sub> capture by anti-sublimation Capture  
336 efficiency and energy consumption for Boiler plants. Seventh International Conference on  
337 Greenhouse Gas control Technologies GHGT7, Vancouver, Canada, 6-9 September 2004
- 338 [11] Tuinier MJ, vanSintAnnaland M, Kramer GJ, Kuipers JAM. Cryogenic CO<sub>2</sub> capture using  
339 dynamically operated packed beds. Chem Eng Sci. 2010;65:114-119.
- 340 [12] Swanson CE, Elzey JW, Hershberger RE, Donnelly RJ. Thermodynamic analysis of  
341 low-temperature carbon dioxide and sulfur dioxide capture from coal-burning power plants.  
342 Physical Review E 2012;86:016103.

- 343 [13] Lively RP, Koros WJ, Johnson JR. Enhanced cryogenic CO<sub>2</sub> capture using dynamically  
344 operated low-cost fiber beds. *Chem Eng Sci* 2012;71:97-103.
- 345 [14] Berstad D, Anantharaman R, Neksa P. Low-temperature CO<sub>2</sub> capture technologies -  
346 Applications and potential. *Int. J. Refrigeration* 2013;36:1403-1416.
- 347 [15] Clodic D, Younes M. A new method for CO<sub>2</sub> capture: frosting CO<sub>2</sub> at atmospheric pressure.  
348 Sixth International Conference on Greenhouse Gas Control Technologies, GHGT-6, Kyoto,  
349 Japan, 1-4 October, 2002. pp.155-160.
- 350 [16] Tuinier, M.J., van Sint Annaland, M., Kuipers, J.A.M.. A novel process for cryogenic CO<sub>2</sub>  
351 capture using dynamically operated packed beds—An experimental and numerical study. *Int J*  
352 *Greenh Gas Con.* 2011;5:694-701.
- 353 [17] Berchowicz DM, Kiiikka D, Mennink BD. Recent advances in Stirling cycle refrigeration.  
354 19th International Congress on Refrigeration Exhibition. August 20-25, 1995, the Hague, the  
355 Netherlands.
- 356 [18] Mennink BD, Goossen WJ. The free-piston Stirling cooling system improving the energy  
357 efficiency of refrigerators. 19th International Congress on Refrigeration Exhibition. August  
358 20-25, 1995, The Hague, The Netherlands.
- 359 [19] Song CF, Kitamura Y, Li SH, Ogasawara KJ. Design of a cryogenic CO<sub>2</sub> capture system  
360 based on Stirling coolers. *Int. J. Greenhouse Gas Control.* 2012;7:107-114.
- 361 [20] Song CF, Kitamura Y, Li SH, Jiang WZ. Parametric analysis of a novel cryogenic CO<sub>2</sub>  
362 capture system based on Stirling coolers. *Environ. Sci. Technol* 2012;46(22):12735–12741.
- 363 [21] Song CF, Kitamura Y, Li SH. Evaluation of Stirling cooler system for cryogenic CO<sub>2</sub> capture.  
364 *Applied Energy* 2012;98:491-501.

365 [22] Berchowitz, DM. Free-Piston Stirling Coolers (1992). International Refrigeration and Air  
366 Conditioning Conference. Paper 171. <http://docs.lib.purdue.edu/iracc/171>.

367

368

369 **Figure captions:**

370 **Fig. 1.** The detailed connection of FPSC-2, cold head and main-freezing tower. (The gray area  
371 represents the vacuum condition of the interlayer in the system.)

372 **Fig. 2.** The detailed configuration of FPSC.

373 **Fig. 3.** The cold head of FPSC with different materials (aluminium and copper).

374 **Fig. 4.** COP variation of FPSC with the root temperature of the cold head under different material  
375 ( $L=180$  mm;  $D=40$  mm).

376 **Fig. 5.** The effect of the material of cold head on the cryogenic temperature ( $L=180$  mm;  $D=40$   
377 mm).

378 **Fig. 6.** COP variation of FPSC with the root temperature of cold head under different length ( $L$ )  
379 (material of cold head is copper;  $D=40$  mm).

380 **Fig. 7.** The relationship of length ( $L$ ) and cryogenic temperature ( $T_c$ ) of the cold head (material of  
381 cold head is copper;  $D=40$  mm).

382 **Fig. 8.** COP variation of FPSC with the root temperature of cold head under different diameter ( $D$ )  
383 (material of cold head is copper;  $L=270$  mm).

384 **Fig. 9.** The relationship of diameter ( $D$ ) and cryogenic temperature ( $T_c$ ) of the cold head (material  
385 of cold head is copper;  $L=270$  mm).

386 **Fig. 10.** COP variation of FPSC with the different ambient temperature ( $T_a$ ) (material of cold head  
387 is copper;  $L=180$  mm;  $D=40$  mm).

388 **Fig. 11.** COP variation of FPSC with different ambient humidity ( $h_a$ ) (material of cold head is  
389 copper;  $L=180$  mm;  $D=40$  mm).

390 **Fig. 12.** COP variation of the FPSCs and system with the root temperature of FPSC-2's cold head  
391 (material of cold head is copper;  $L=180$  mm;  $D=40$  mm). COP-1, COP-2, COP-3 and COPS  
392 represent the coefficient of performance for FPSC-1, FPSC-2, FPSC-3 and the whole system,  
393 respectively.

394

395

396

397

398

399

400

401

402

403

404

405

406

407

408

409

410

411

412

413

414

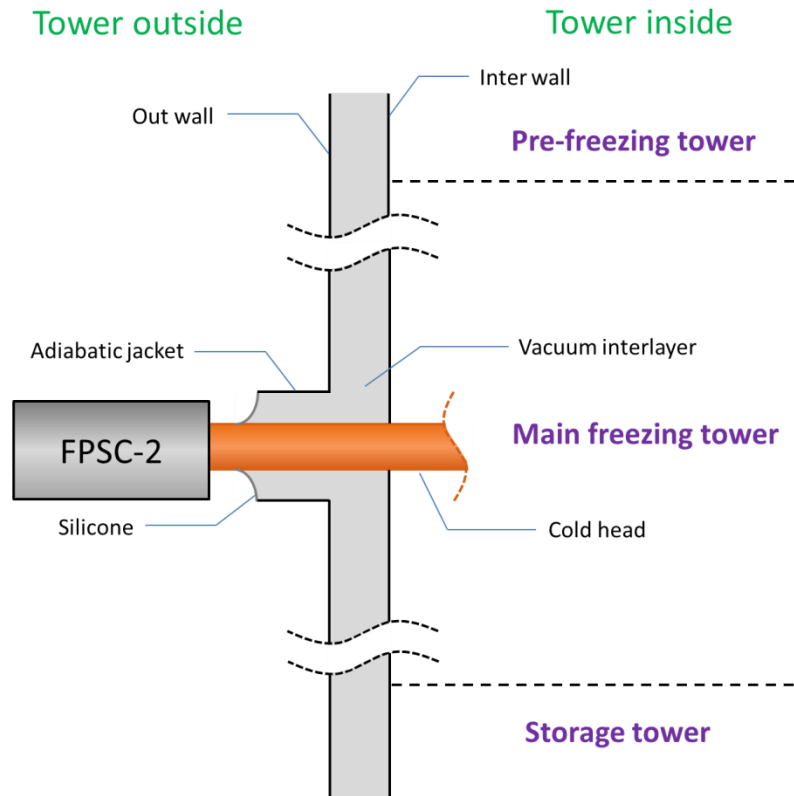
415

416

417

418

419



420

421 **Fig. 1.** The detailed connection of FPSC-2, cold head and main-freezing tower. (The gray area  
 422 represents the vacuum condition of the interlayer in the system.)

423

424

425

426

427

428

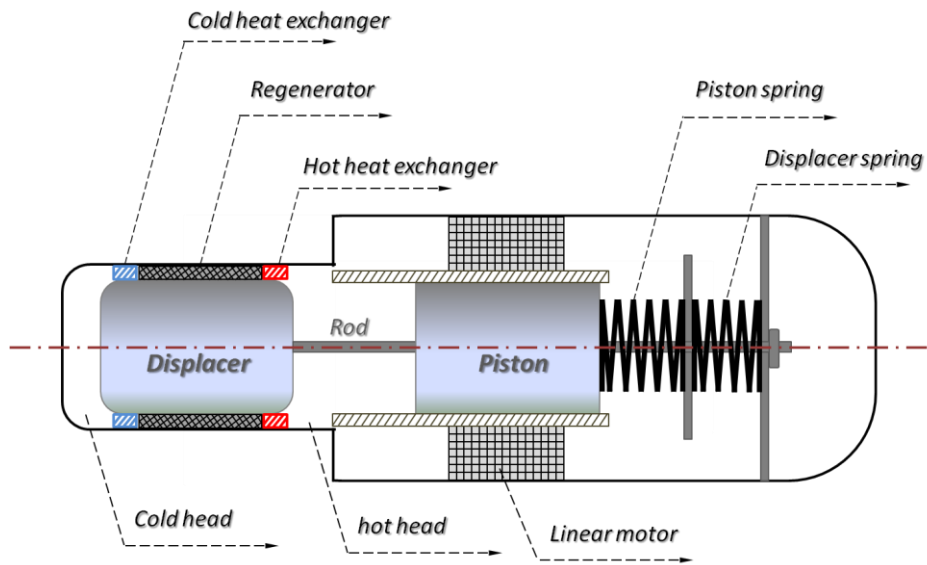
429

430

431

432

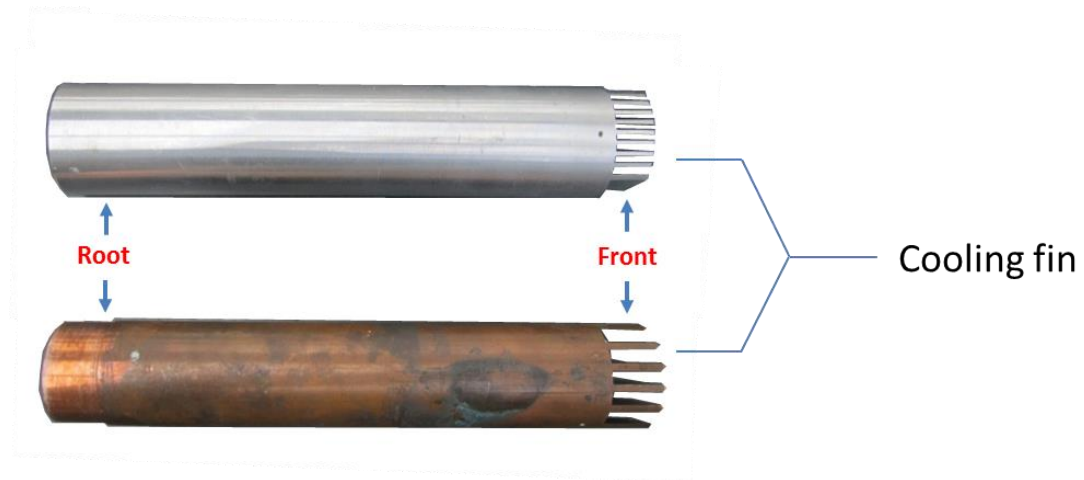
433



434

435 **Fig. 2.** The detailed configuration of FPSC.

436



437

438 **Fig. 3.** The cold head of FPSC with different materials (aluminium and copper).

439

440

441

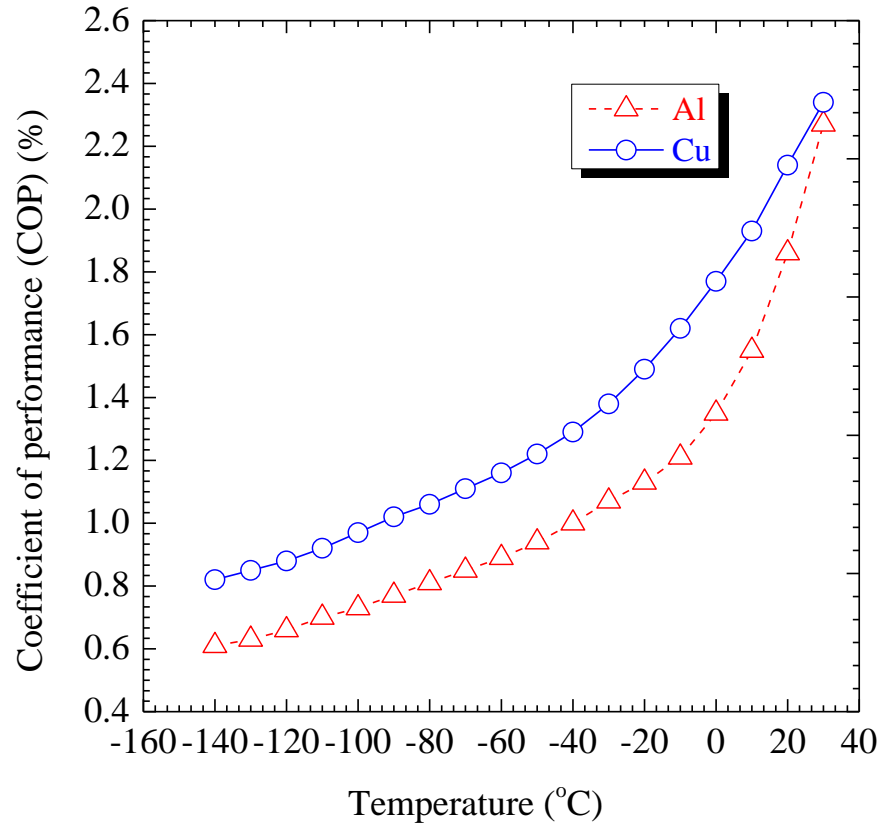
442

443

444

445

446



447

448

449 **Fig. 4.** COP variation of FPSC with the root temperature of the cold head under different material

450 (L=180 mm; D=40 mm).

451

452

453

454

455

456

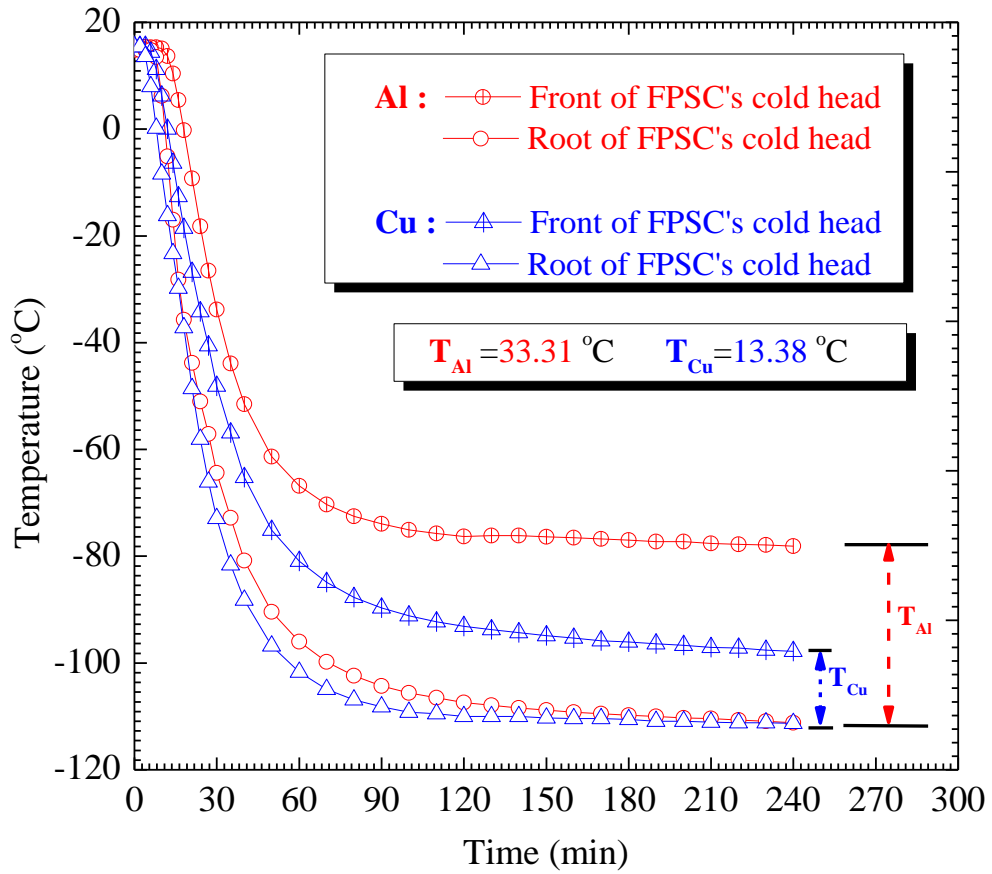


457

458

459

460



461

462

463 **Fig. 5.** The effect of the material of cold head on the cryogenic temperature (L=180 mm; D=40

464 mm).

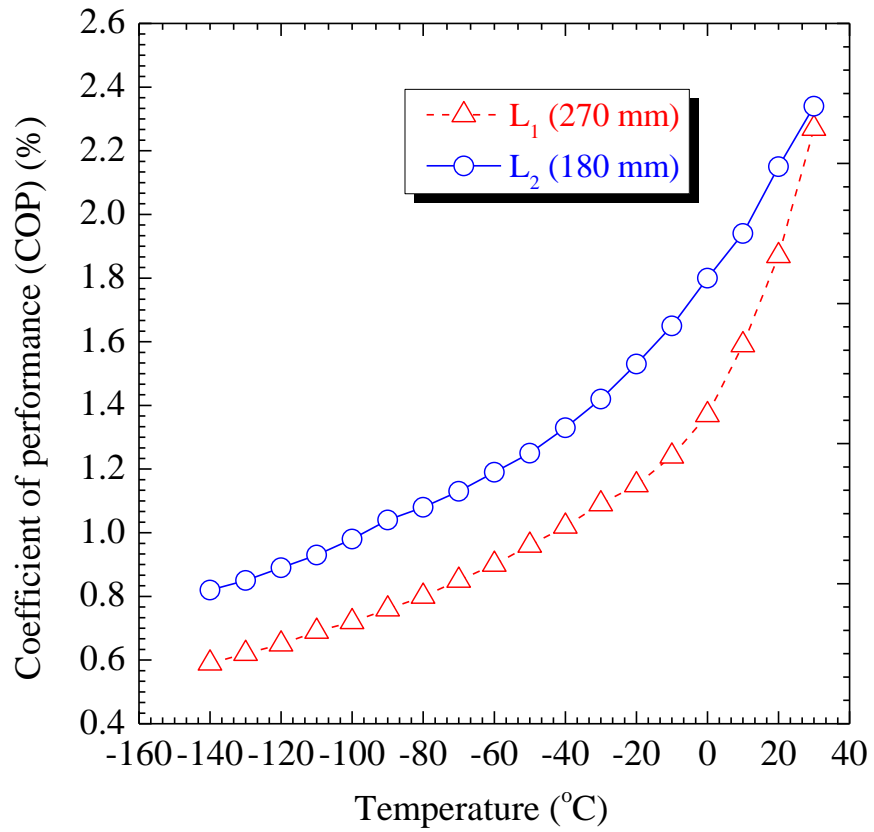
465

466

467

468

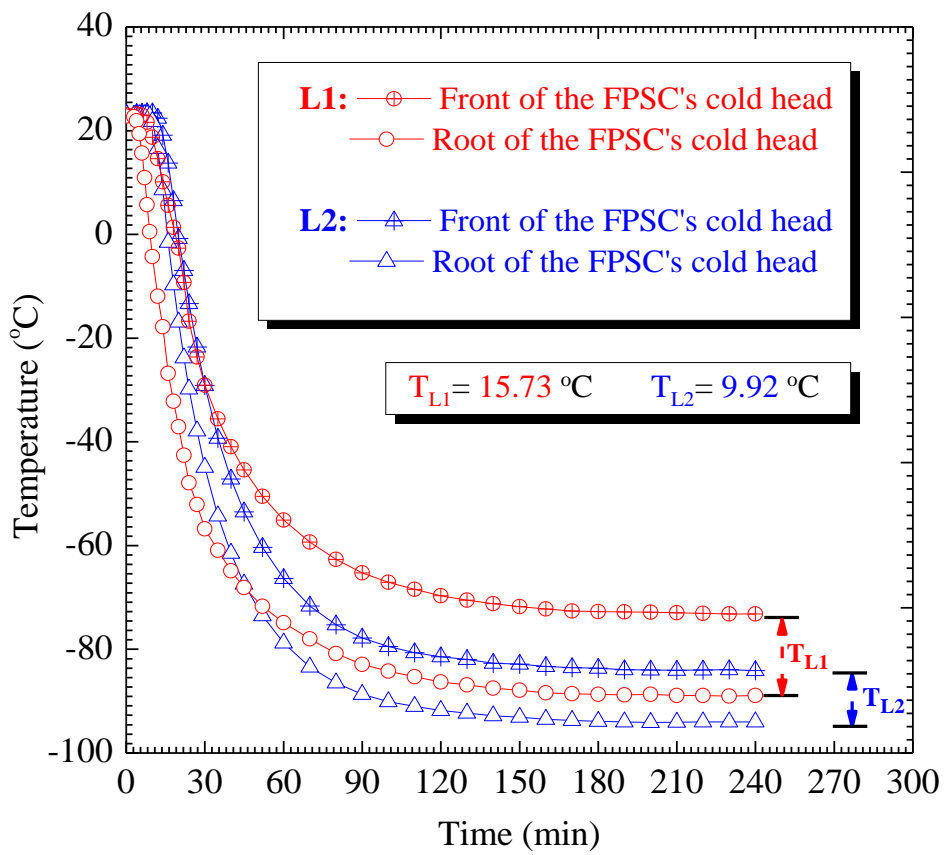
469  
470  
471  
472  
473  
474  
475  
476



477  
478  
479  
480  
481

**Fig. 6.** COP variation of FPSC with the root temperature of cold head under different length ( $L$ ) (material of cold head is copper;  $D=40$  mm).

482  
483  
484  
485  
486  
487  
488  
489  
490  
491



492  
493

494 **Fig. 7.** The relationship of length ( $L$ ) and cryogenic temperature ( $T_c$ ) of the cold head (material of  
495 cold head is copper;  $D=40$  mm).

496

497

498

499

500

501

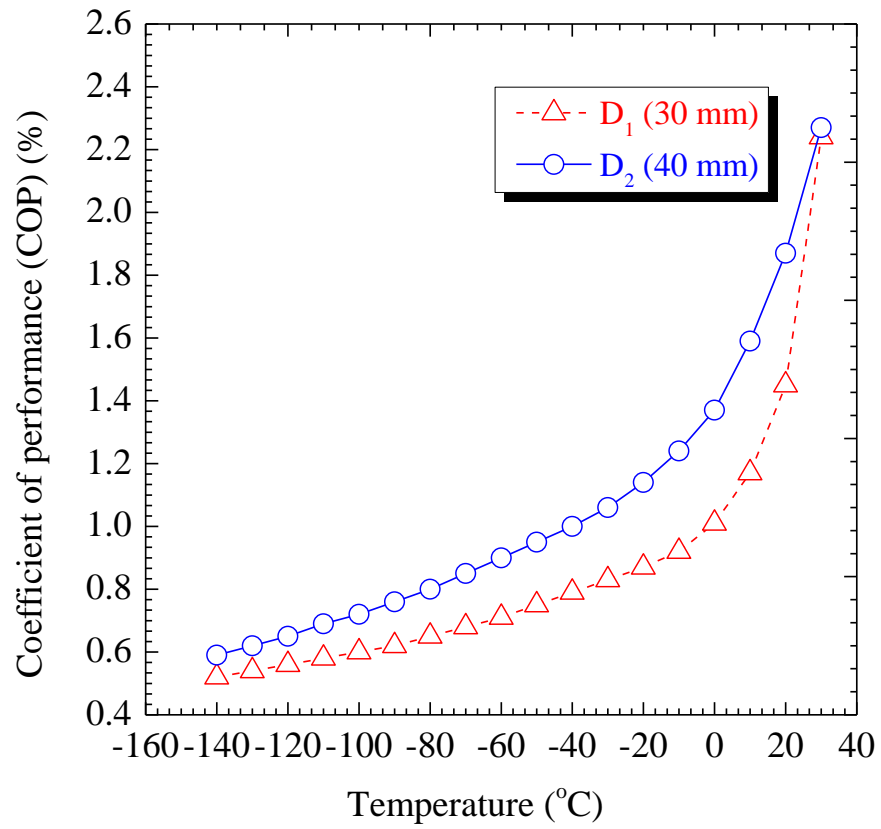
502

503

504

505

506



507

508

509 **Fig. 8.** COP variation of FPSC with the root temperature of cold head under different diameter ( $D$ )

510 (material of cold head is copper;  $L=270$  mm).

511

512

513

514

515

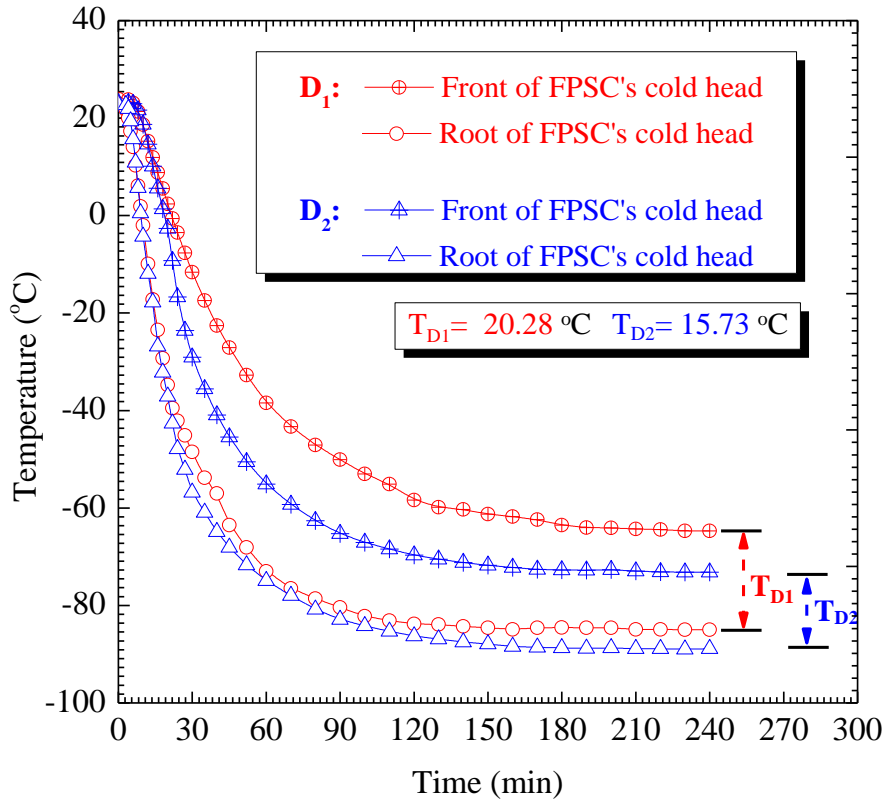
516

517

518

519

520



521

522 **Fig. 9.** The relationship of diameter ( $D$ ) and cryogenic temperature ( $T_c$ ) of the cold head (material  
523 of cold head is copper;  $L=270$  mm).

524

525

526

527

528

529

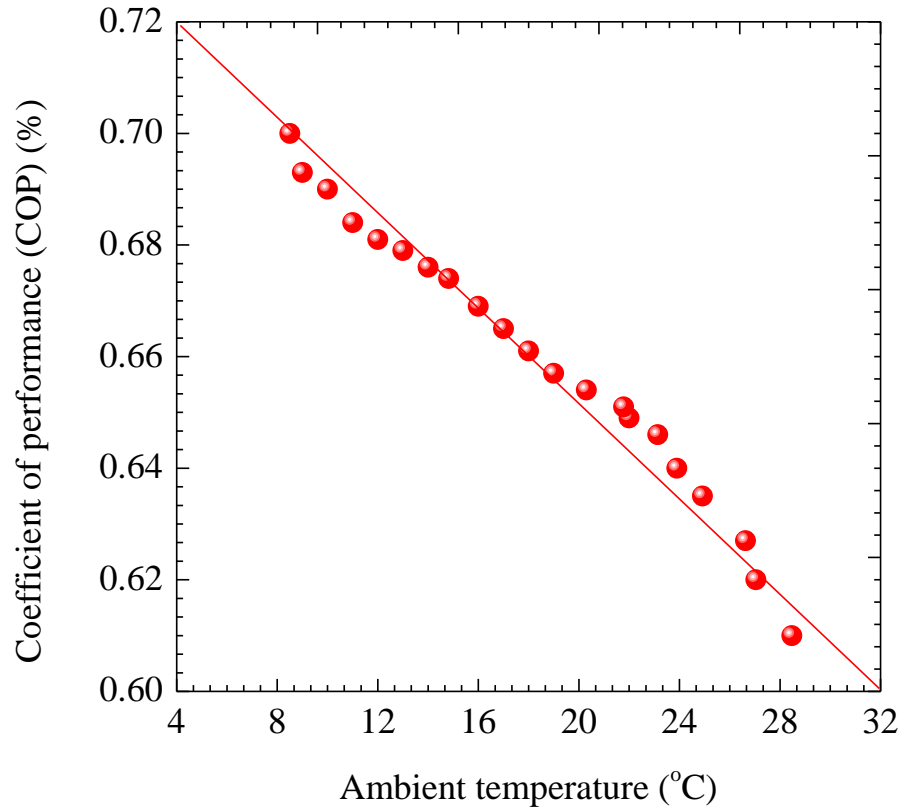
530

531

532

533

534



535

536

537 **Fig. 10.** COP variation of FPSC with the different ambient temperature ( $T_a$ ) (material of cold head

538 is copper; L=180 mm; D=40 mm).

539

540

541

542

543

544

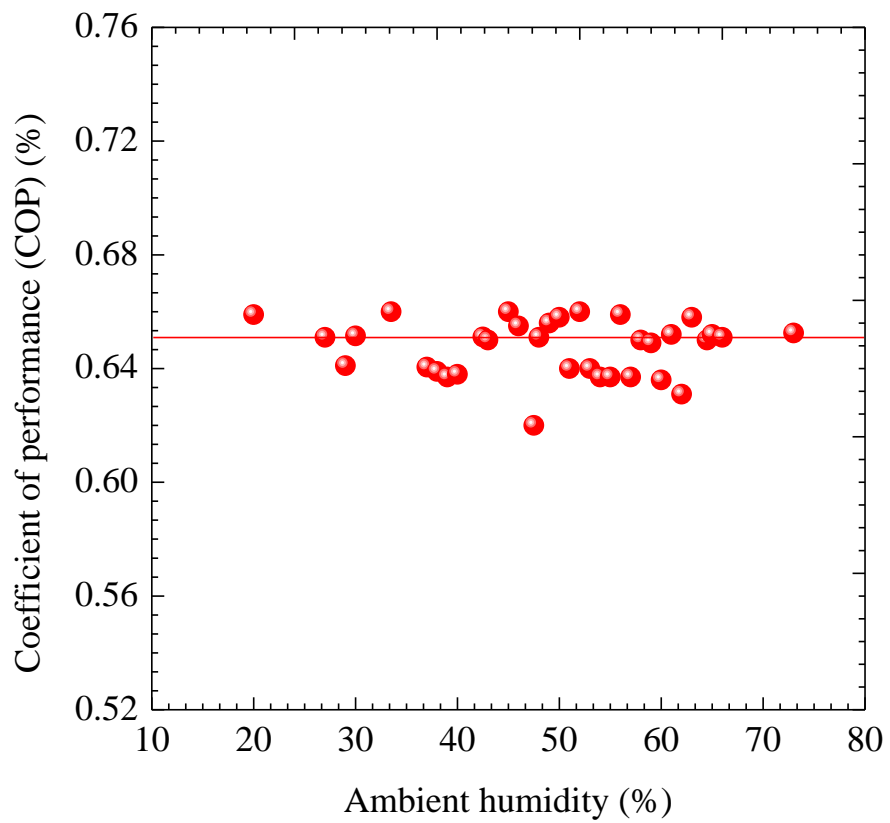
545

546

547

548

549



550

551

552 **Fig. 11.** COP variation of FPSC with different ambient humidity ( $h_a$ ) (material of cold head is

553 copper; L=180 mm; D=40 mm).

554

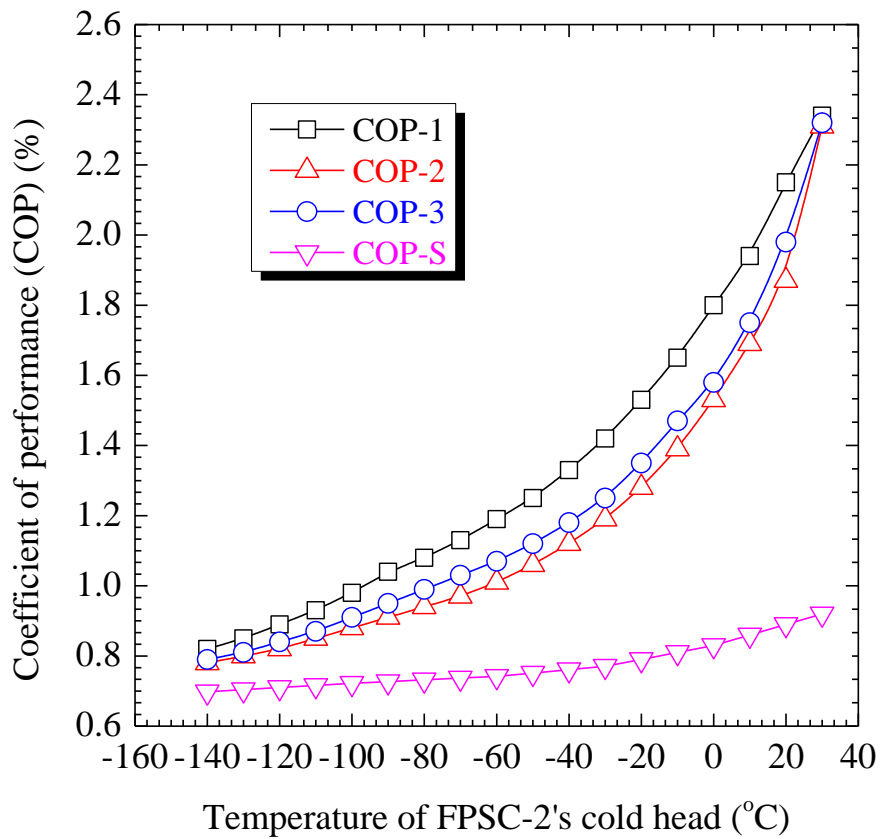
555

556

557



558  
559  
560  
561  
562  
563  
564



565  
566

567 **Fig. 12.** COP variation of the FPSCs and system with the root temperature of FPSC-2's cold head  
568 (material of cold head is copper; L=180 mm; D=40 mm). COP-1, COP-2, COP-3 and COPS  
569 represent the coefficient of performance for FPSC-1, FPSC-2, FPSC-3 and the whole system,  
570 respectively.

